Carbonates and Evaporites (2020) 35:53
https://doi.org/10.1007/s13146-020-00589-2

ORIGINAL ARTICLE

Snow cover monitoring by remote sensing and evaluating melting water effects on karstic springs discharges (a case study from Lasem area)

Abdollah Shamsi[1] · **Gholam Hossein Karami**[1] · **Daniel Hunkeler**[2]

Accepted: 30 April 2020 / Published online: 16 May 2020

Abstract
Snowfall is the dominant form of precipitation in high mountainous areas and its driving melt water has an indispensable role in the hydrological cycle and groundwater recharge, particularly in karstic landscapes with high infiltration capacity. Monitoring snow cover area (SCA) and its melting process is essential for the investigation of climatic variables, hydrology, hydrogeology, and water resource management. Prodigious advances of satellite imaginary technology in the past decades made it possible to monitor spatiotemporal distribution of snow and its melting process. In this research, SCA was investigated using cloud-free images of Landsat-8 from December 2014 to June 2016 and Sentinel-2 from November 2015 to June 2016 at Lasem area (north of Iran) by normalized difference snow index. Simultaneously, the discharges of the main karstic springs were monitored over May 2015 to June 2016. The catchment subdivided into three sub-zones based on the hydrogeological characteristics and snow melting time. Fractional SCA time series within each subdomain used to develop snow melting curve in each subzone. Comparison of melting peaks between the 2014–2015 and 2015–2016 water years shows that melting shifted in average 20 days later in 2016 at north-facing subdomains. North-facing slopes show quite fast transmitting time (20–35 days) of the peak snowmelt to the springs, while the south-facing springs are more silent to the recharge pulses (70–80 days), indicating a higher degree of karstification in north-facing domains. More concentrated snowmelt in 2016 led to increasing peak flow by an average of 15% in the springs fed by north-facing domains.

Keywords Lasem · Snowmelt · Landsat-8 · Sentinel-2 · Karst spring · NDSI

Introduction

Snow is the dominant form of the precipitation in the mountainous areas, which accumulates during the cold weather conditions (Smith et al. 2017). Moreover, it acts as a temporary water storage in the high mountainous areas (Schmieder et al. 2016). Mountain snowpack provides water resources for nearly 1.5 billion of the world's population and is critical for arid and semiarid regions water supply (Barnett et al. 2005). Snowmelt is a significant component of the hydrologic cycle, and it is the main source of recharge to the high-altitude aquifers (Flerchinger et al. 1992; Gusev and Nasonova 2014; Tedesco et al. 2014), especially in karst domains due to high infiltration capacity (Radulovic et al. 2012; Bonacci and Andrić (2015); Hartmann et al. 2017). Spatiotemporal variability of the snow covers and its deriving melt water play an important role in availability of water for downstream users (Smith et al. 2017). In addition to the water that drives from snowpack, it has a capacity to absorb and temporary store rainwater that occurs in the early snowmelt season (Schmieder et al. 2016).

Owing to the difficulty of installing, maintaining, and monitoring instruments, investigating of hydrologic and hydrogeological variables in the high mountainous areas is challenging (Brown et al. 2014). Brilliant developments in the aerospace technology and possibility of acquiring high-resolution images by satellites made it possible to achieve the high spatial and temporal resolution data. Spatially continuous information delivered by image processing of remote sensing data allow the researchers to monitor the snow cover area over the melting

✉ Gholam Hossein Karami
a.shamsi@shahroodut.ac.ir; a.shamsi2012@gmail.com

[1] Faculty of Earth Sciences, Shahrood University of Technology, Shahrood, Iran

[2] Center for Hydrogeology and Geothermics (CHYN), University of Neuchâtel, Neuchâtel, Switzerland

period. Application of the satellite images to monitor the snow cover and snow sublimation has been examined in the past decades (Rango et al. 1996; Bormann et al. 2012; Hall et al. 2012; Crawford et al. 2013; Brown et al. 2014; Hall et al. 2015; Fassnacht et al. 2016; Kääb et al. 2016; Fassnacht et al. 2017). Temporal evaluation of snow cover friction for a distinct area delivers information about the sublimation time and snowmelt rate that refers to snowmelt curve (Hall et al. 1995). Snow cover can be evaluated by optical/thermal and microwave remote sensing. Scientists from many different regions investigated the effect of the snowmelt on the quality and quantity of groundwater and the stream flow (Flerchinger et al. 1992; Deng et al 1994). Simulating of snowmelt at the forest hill slope in the Sierra Nevada Mountains of California show fast groundwater level change due to the snowmelt (MacDonald 1987). Monitoring of the snowmelt and water level in piezometers located 135 m downslope indicates 3–4 days' delay to observe the melting effect (Flerchinger et al. 1992).

Karstic aquifers are highly heterogeneous and anisotropic systems (Padilla et al. 1994; Bakalowicz 2005; White 2007; Bonacci and Andrić (2015); Poulain et al. 2015). Complex topography in the mountainous areas will affect the distribution of the precipitation that subsequently imposes extra heterogeneity to these aquifers. Karst terrains with developed conduit systems almost react quickly and strongly to the high-amount precipitation events and snowmelt (Kavousi and Raeisi 2015). However, in poorly karstified terrains regulatory effects of aquifer dilutes the input signals and makes it nearly impossible to distinguish signals in the spring outflow (Miao et al. 2014). Snowmelt process occurs in the whole of the spring's catchment and may provide an insight to the degree of karstification, attenuation characteristic of the aquifer, and time lag between the pick of the snowmelt and springs high flow condition. Remote sensing can deliver spatially continuous information about snow cover in reliable temporal and spatial resolutions.

The main aim of this research is to apply the remote sensing for quantifying and monitoring of the snowmelt in the Lasem area as well as examining the effect of snow sublimation on karst springs discharge between 2015 and 2016. Moreover, it is aimed to figure out the time lag using the relation between snowmelt and springs discharge fluctuations specifically using the transient time of the peak snowmelt to the springs. The final aim of this research will be comparing the results of snowmelt between the Landsat-8 and Sentinel-2 dataset.

The study area

Lasem watershed is situated at Haraz basin in elevated part of Central Alborz Mountain, 85 km northeast of Tehran (capital of Iran). The study area is extended between 36° 39′ 30″ N to 36° 51′ 40″ N and 52° 1′ 00″ E to 52° 21′ 00″ E (Fig. 1). The entire catchment area has relatively steep topography with an average slope of 38°.

The elevation ranges from 4250 m above sea level (a.s.l.) at the headwaters to 1500 m a.s.l. at the outlet of the Lasem watershed. Geologically, the study area belongs to the Central Alborz Mountain Range with continuous folded geological formations in NW–SE direction and several active faults parallel or sub-parallel to the main structures (Berberian and Yeats 1999). The geological units in stratigraphic succession are from the Triassic to the Quaternary (Fig. 2). Carbonate formations cover about 35% of the Lasem watershed and remaining 65% is covered by non-carbonate (mainly tuff and shale) and alluvial deposits. Vegetation on limestone outcrops is infrequent, but it is relatively more concentrated on debris, alluvial deposits, and other rock types.

The hydrologic cycle of Lasem high-altitude watershed is characterized by snow accumulation from late autumn, winter, and early spring that is following by a snowmelt runoff period during late spring and early summer. The mean amount of annual precipitation based on the 27 years' data of Polour meteorology station varies from 430 to 850 mm/year with a mean of 625 mm/year (Shamsi et al. 2019). The annual precipitation rises with elevation and shows about 5 mm increase for every 100 m of elevation (Khalili 1973). With regard to the amount of precipitation, December to February receives the highest amount of precipitation, while it is minimum during summer. The annual average of the maximum, mean, and minimum temperatures are 15.76, 9.98, and 4.13 of °C, respectively. At this area, air temperature at late autumn, winter, and early spring is low as the mean air temperature is below zero. The presence of snow at some part of the deep valleys in the late summer suggests cold condition even in the summer.

Lasem River drains the study area and its discharges in peak flow and base flow conditions are 15 and 0.8 m^3/s, respectively. Streamflow from September to November is predominately base flow, while it is flooded by snowmelt from March to June. However, it has the potential for storm flow from heavy rainfall. Karst springs are the main source of water in the base flow condition.

Tectonic structures lead to the partitioning of the aquifers to the Southern sector (SS) and Northern sector (NS) that are drained by 10 and 5 main karst springs, respectively (Shamsi et al. 2019). Discharge of the springs ranges from 2500 to 20 L/s in the peck flow time and 200 to 6 L/s in the base flow condition. Karst springs catchment area in SS are dominated by north-facing slope (NFS), while karst springs catchment area of NS dominated by south-facing slope (SFS). Springs of NS dominantly feeding by the SFS showing only one recession coefficient while discharging springs from SS dominantly recharges by NFS having 2 or 3 recession coefficients (Table 1), indicating higher karstification degree in

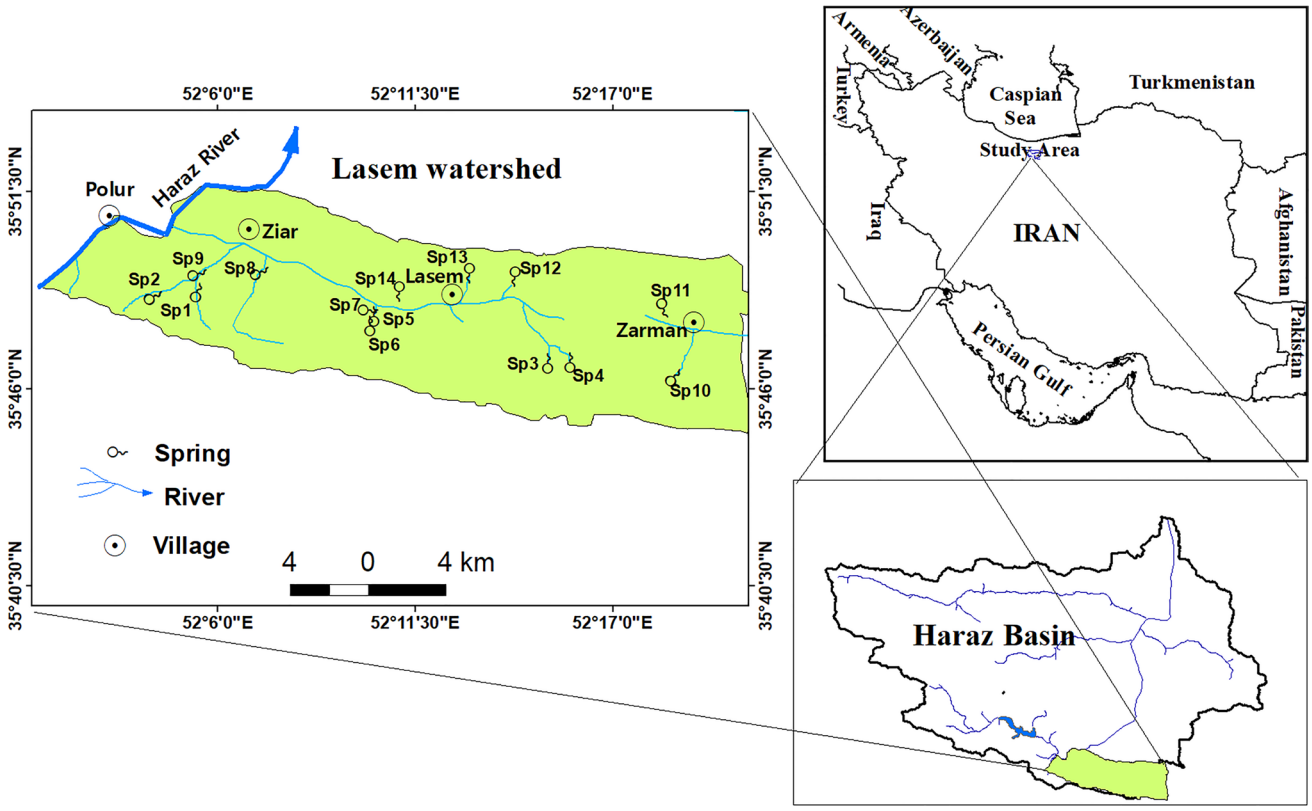

Fig. 1 Geographical location of the study area

the southern sector. Likewise, springs discharge and their variabilities in SS are very high, whereas those are relatively small for springs of NS, indicating higher degree of karstification is higher in NFS than SFS (Shamsi et al. 2019).

Data and methods

Data

The passive remote sensing data were used in this research for monitoring of the temporal and spatial distribution of SCA and investigating the snowmelt driving water effect on the karst springs discharge in Lasem area. In this regard, cloud-free images of Landsat-8 from December 2014 to June 2016 and Sentinel-2 from November 2015 to June 2016 (spatial resolutions of 30 m for Landsat-8, 20 m for Sentinel-2) were selected to use. The data were downloaded from available Landsat-8 and Sentinel-2 imagery archives (Earth Explorer (2016), European Space Agency (ESA) (2016) web sites). Temporal resolutions of the Landsat-8 and Sentinel-2 images are 16 and 10 days, respectively; however, in overlapped area of images, this may be lower. Unluckily, many images are excluded due to cloud contamination issues.

An extensive field survey is carried out from March 2015 to June 2016 for collecting the springs discharge data and investigating the hydrogeology of the study area. Data collection was carried out by regular biweekly (April 2015 to September 2015), measuring of discharge during the recession period, and by monthly in the base flow condition (October 2015 to June 2016). The flow meter is used for measuring of the flow velocity of high discharges, and low discharge rates are measured using volumetric method. The characteristics of the main karst springs are summarized in Table 1.

Methods

Karst landforms almost are not resilient to the imputing pulses (Shamsi et al. 2019) owning to the high hydraulic conductivity as a result of the secondary porosity development (Bonacci 1993; Fiorillo and Guadagno 2012). Snow sublimation produces a huge pulse that could be observed in karst springs discharge. In this regards, Landsat-8 and Sentinel-2 data are used for the detection of SCA and the investigation of melting trend. QGIS "which is an open source software" is used to read and manipulate the data. Raw unprocessed digital numbers are converted to the sensor radiance values using Landsat-8 and Sentinel-2 calibration

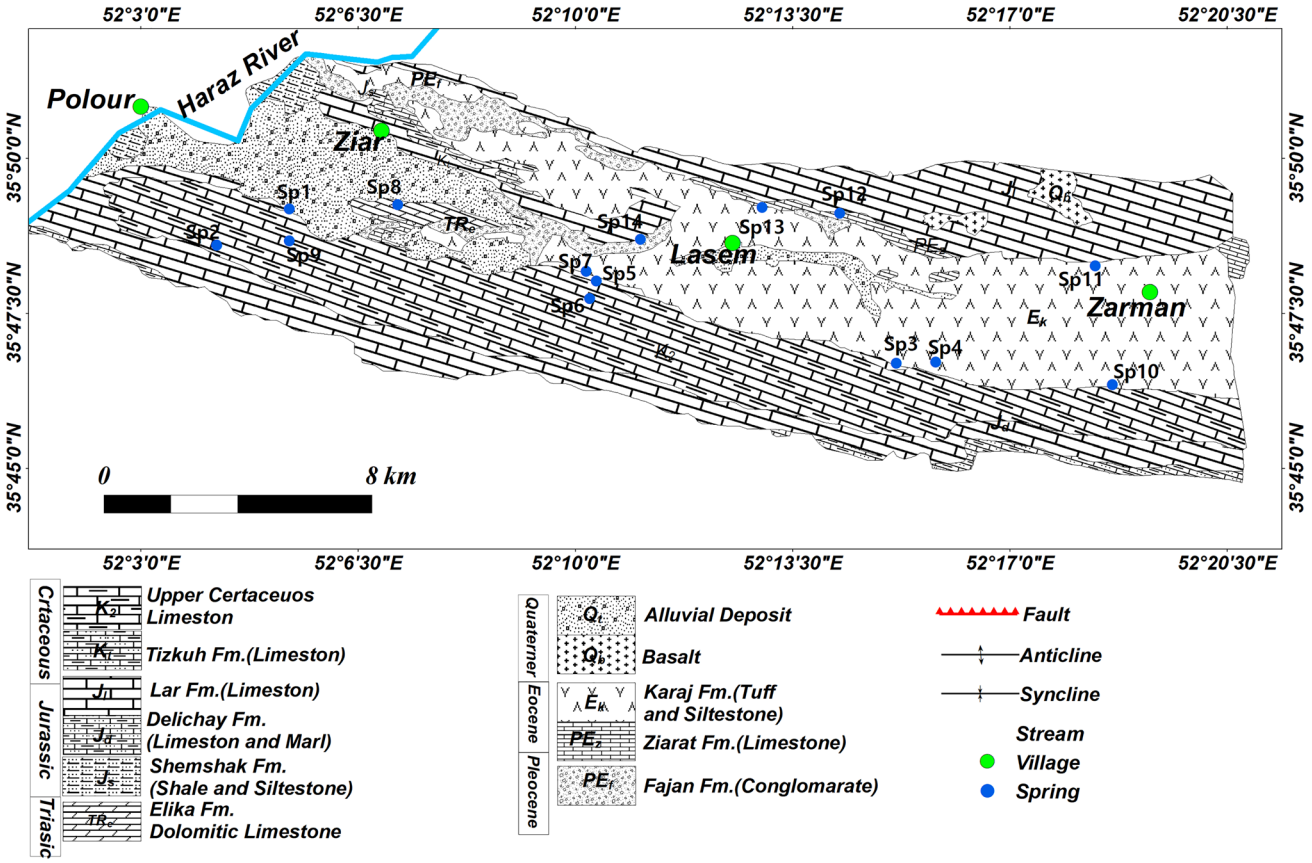

Fig. 2 Geological map of the study area (Modified after Emami and Babakhani 1997)

Table 1 The discharges value of karst springs in Lasem watershed (after Shamsi et al. 2019)

Spring name	Abbreviation on the map	Dominant feeding slope	Q_{min} (L/s)	Q_{avg} (L/s)	Q_{max} (L/s)	CF (%)[a]	α_1[b]	α_2	α_3
Shikh Alikhan2	Sp1	Northern	125	611	2500	109.2	0.003	0.054	0.01
Shikh Alikhan1	Sp2	Northern	150	300	750	54.9	0.005	0.033	0.004
Angemar	Sp3	Northern	75	277	450	62.2	0.004	0.013	–
Shamsin	Sp4	Northern	65	105	140	34.2	0.003	0.014	0.002
Abmorad1	Sp5	Northern	17	90	320	40	0.005	0.05	0.012
Abmorad 2	Sp6	Northern	3	233	1500	163.2	0.03	0.061	0.035
Zehro	Sp7	Northern	230	850	2300	46.5	0.009	0.041	–
Ab morad3	Sp8	Northern	0.3	24	70	119.4	0.019	0.003	0.006
Myanroud	Sp9	Northern	55	65	100	31.4	0.002	0.036	–
Rakhsh	Sp10	Northern	210	391	600	28.2	0.002	0.006	0.001
Zardeh	Sp11	Southern	28	42	60	6.61	0.001	–	–
March	Sp12	Southern	35	96	200	38.7	0.007	–	–
Lalehgon	Sp13	Southern	16	33	75	46.3	0.007	–	–
Zarincheshmeh	Sp14	Southern	1	9.5	40	104	0.019	–	–

[a]Coefficient of discharge variation

[b]Recession coefficient

coefficient. Then it is converted to planetary reflectance value. Ground control points were used for the evaluation of the image positioning accuracy.

Snow is highly reflective in the visible part of the spectrum and highly absorbing in near infrared and shortwave infrared parts of the electromagnetic spectrum (Dietz et al. 2012, 2014). Therefore, the snow cover extents are identified better using visible and infrared/shortwave parts of the wavelength. Normalized difference snow index (NDSI), which was developed for the detection of snow, is the normalized difference between visible green and shortwave infrared bands (Hall et al. 1995). Generally, the NDSI is calculated in this form: (very high visible (VIS) − shortwave infrared (SWIR))/(VIS + SWIR) (Dozier 1989; Rittger et al. 2012; Macander et al. 2015). Since cloud has high reflectance in near infrared (NIR) and SWIR bands, application of the NDSI ratio allows discrimination between snow and cloud, moreover to some extent it allows the removal of shadow effects on the mountainous area. NDSI was calculated for Landsat-8 bands 3(0.53–0.59 µm) and 6 (1.57–1.65 µm) and Sentinel-2 bands 3 (0.54–0.58 µm) and 11 (1.57–1.66 µm), utilizing the method developed by Hall et al. (1995). High value of NDSI represents the snow, while pixels without snow tend to have much lower values (Dietz et al. 2012). Based on the literature (e.g., Hall et al. 1995; Miao et al. 2014; Egbers, 2016), NDSI ≥ 0.4 is considered as snow coverage. However, this threshold is variable in a forested area. It should be noted that this algorithm only works for pixels dominated by snow cover (Hall et al. 2002). Changes of snow cover on 16 days (Landsat-8 images) and 5 days (Sentinel-2) temporal resolutions are used to drive the snow cover depletion curve, which represents the snowmelt process. Snow cover depletion curves were developed by dividing the SCA to the whole of the subdomains area.

Based on the hydrogeological framework including the dominance of the feeding slope direction, springs discharge recession, and snowmelt trend, Lasem carbonate formations were subdivided into three zones (Fig. 3). The south-facing slope (SFS), lower north-facing slope (LNFS), and higher north-facing slope (HNSF) are the main hydrogeological units. The total discharges from each zone are the summation of all the springs included in that zone.

Results

Snow cover maps

Using the NDSI index with visual inspection of multispectral color composites, snow cover maps were derived from Landsat-8 (December 2014 to the June 2016) and Sentinel-2 (November 2015 to the June 2016) images. A pixel is classified as snow if NDSI ≥ 0.4, visible bands reflectance (Landsat-8 band 3 and Sentinel-2 band 3) was greater than 0.10, and near-infrared bands reflectance (Landsat-8 band 3 and Sentinel-2 band 11) was greater than 0.11, otherwise it classified as the snow-free surface. Using this method, totally 21 snow maps were created from December 2014 to June 2016 and from November 2015 to June 2016 by Landsat-8 and Sentinel-2 images, respectively. SCA monitoring of two consecutive years with cloud-free scenes indicates that the majority of the land surface at high latitude is covered with snow during winter; however, some snow-free surfaces exist (Fig. 4). Considering SCA against slope direction and elevation shows that the slope direction has more effect than the elevation as the higher elevated parts of south-facing slopes (SFSs) lose the snow earlier than the lower elevated area with NFS. The SFS shows higher variability in SCA than NFS.

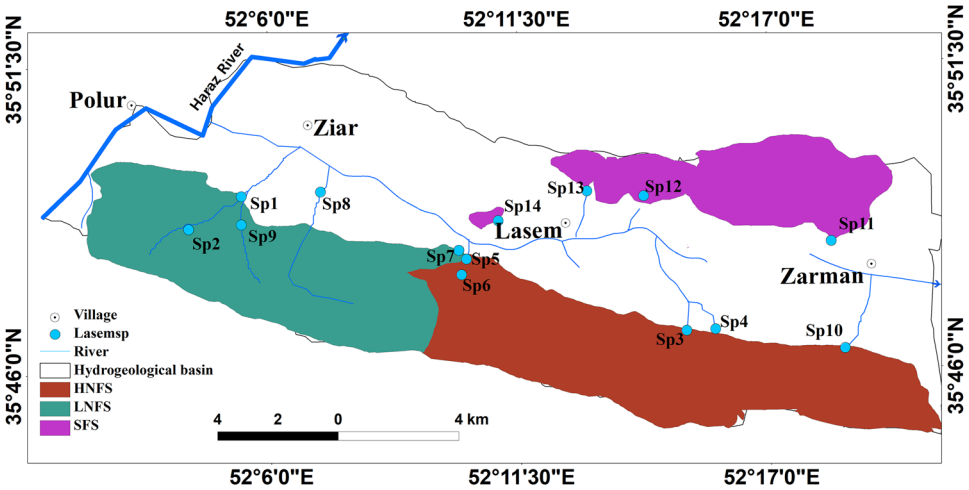

Fig. 3 Hydrogeological units of the Lasem basin

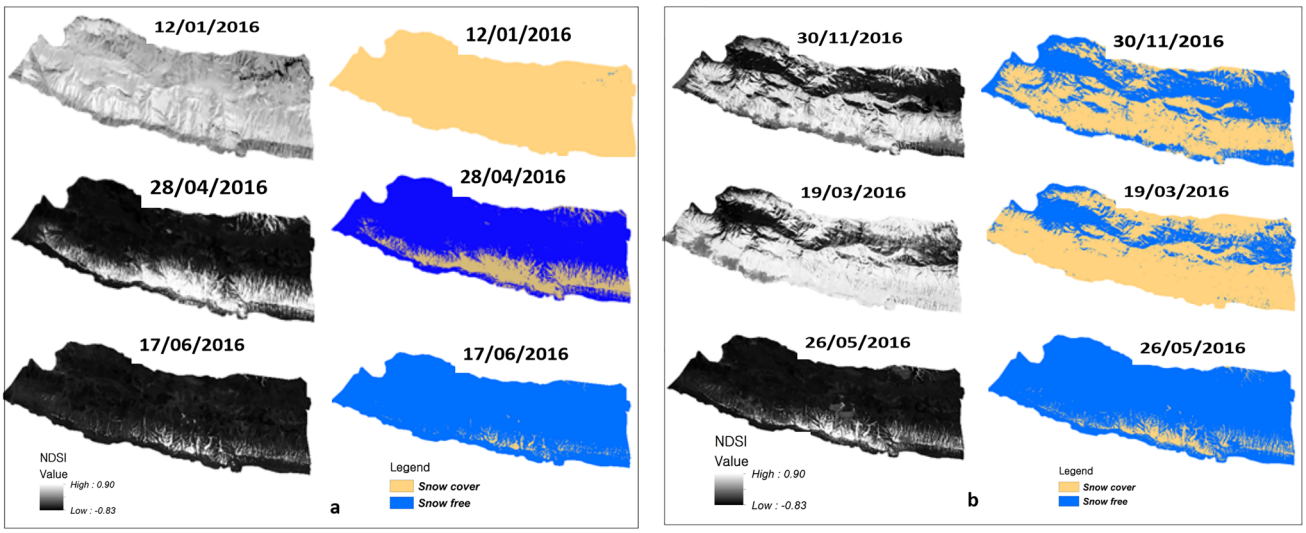

Fig. 4 An example NDSI and snow maps derived from Landsat-8 (**a**) and Sentinel-2 (**b**) images

Snowmelt curves

Snow cover friction (SCF) is determined for the whole catchment and subdomains by plotting the ratio of SCF against time. Lasem basin SCFs from December 2014 to June 2016 by Landsat-8 images and from November 2015 to June 2016 by Sentinel-2 images are shown in Fig. 5. SCFs derived from both Landsat-8 and Sentinel-2 images are showing a general consistency with each other. However, some small disagreements exist which could be explained either by the early melt of snow in SFS or higher sensitivity of the Sentinel-2 images owing to higher spatial resolutions. As can be seen, the study area in 2016 was almost covered by snow for more than 2 months, while such a coverage of snow did not exist in 2015.

The majority of snow melts during May; however, in higher elevated NFS snow preserved until June and some deep valleys were covered by snow cover all year round. Although the cumulative amounts of snowfall in the following years are the same, there is a distinct delay (20 days) in the peak melt time in 2016 in comparison to 2015. The cumulative amounts of the snow equivalent water (from December to April) of two successive hydrologic years (2014–2015 and 2015–2016) are nearly the same (415.3 and 393.8 mm, respectively) (Fig. 6). The peak of total discharge from the catchment shows rising by ~ 14% (Fig. 5) due to more intense snow sublimation in the second hydrologic year (2015–2016).

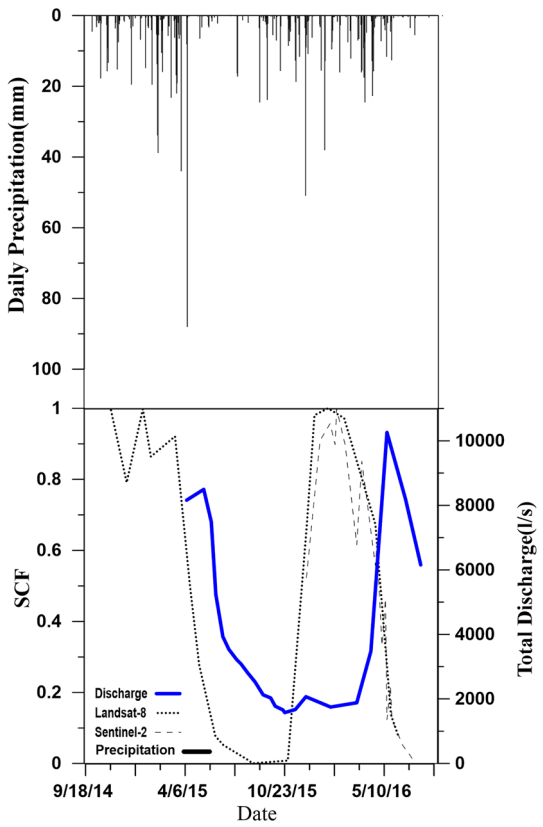

Fig. 5 Trend of snowmelt over the whole of the basin in two years

Snowmelt in sub-zones

The SCF of each sub-zone extracted from both Landsat-8 and Sentinel-2 are shown along with the total discharge of springs in each sub-zone (Fig. 7a–c). The south-facing subzone shows no obvious change in both snowmelt and karst springs discharge in the two successive years. Snowmelt have nearly the same starting time and duration though in 2014–2015 there are fluctuations due to limited early melt

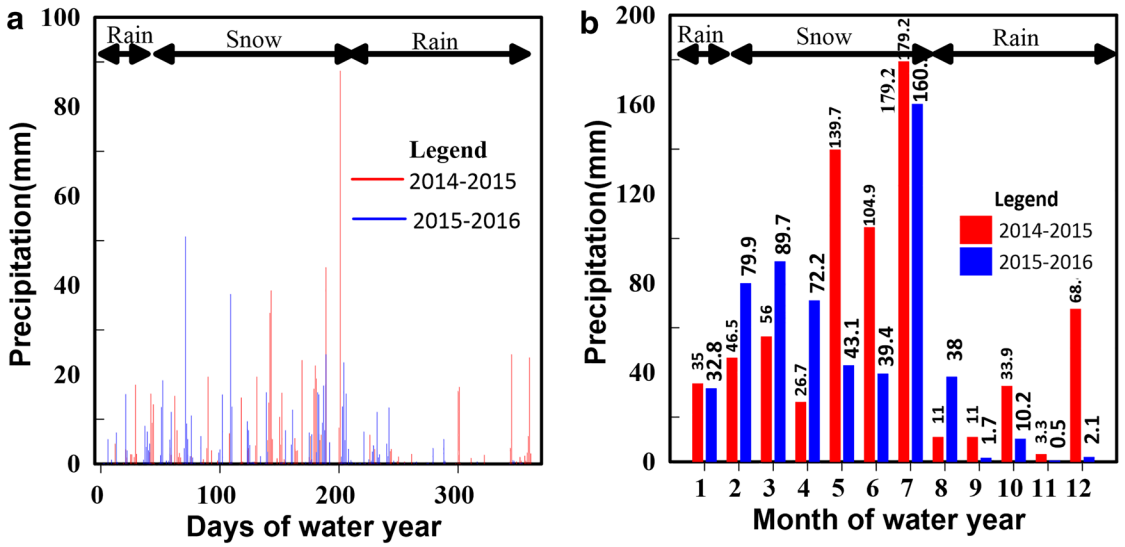

Fig. 6 Precipitation distribution over the monitoring period; daily (**a**) and monthly (**b**)

process (Fig. 7a). A comparison of the dominant snow melting period and peak of discharge in south-facing sub-zone indicates that it takes nearly 70–80 days to observe the peak melting effects on the cumulative peak discharge of the springs (Fig. 7a).

Lower north-facing sub-zone is covered by the snow nearly whole of the winter and melting process takes nearly 70–80 days (Fig. 7b). This zone shows quite a low residence time and springs discharge responses to the snowmelt by 20–35 days. The HNFS is covered by snow more than the other zones and snowmelt starts later in comparison to other sub-zones (Fig. 7c). Melting process lasts nearly 100 days and dominant melting is more concentrated than the other two sub-zone. The time lag between the peak of snowmelt and peak discharge is about 20–35 days, which is similar to the LNFS.

Comparing total springs discharges of both sub-zones in 2014–2015 and 2015–2016 shows nearly 15% increase of the peak discharges in the second year, while there is no significant change in precipitation amount (415.3 and 393.8 mm, respectively) (Fig. 6).

Discussion

Tracers are valuable tools that widely used in hydrogeological investigation especially in karst landforms. Application of natural or artificial tracers is almost expensive and labor demanding. Snowmelt pulses are valuable cost-effective tracer which occurs through the whole of the spring catchment. Brilliant developments in technology of acquiring remote sensing images and its processing provide valuable data for mapping SCA and its melting trend, especially in basin scale. However, the mapping of snow cover suffers from image acquisition frequency, snowfall during the imagining time, cloud cover over mountainous terrain, and different spectral and spatial resolutions (Hall et al. 2012). Using two datasets is applicable to overcome some of these problems and gaps could be filled by each other.

Freely available images of Landsat-8 and Sentinel-2 with moderate spatial resolutions and respectively 16 and 10 days of temporal resolutions are providing acceptable data to map SCR and drivation of melting curve.

SCA monitoring results of the two consecutive years indicate that the majority of the land surface at high latitude is covered with snow during whole of the winter; however, some snow-free surfaces do exist due to reworking of snow by wind or early melt of SFS (Fig. 4). The acquired results by two satellites correlate well with each other, indicating the dominance of snowmelt in May in the study area.

The results of the two consecutive years of springs discharge monitoring and time series analysis of the SCF show an inverse relationship between the SCA and discharge of the springs with low residence time karst aquifers. By reducing the SCA, the springs discharge tends to increase. According to the field measurements results, the karst springs cumulative peak discharge of NFS increases by 15% in 2015–2016 in comparison to 2014–2015. Raise of peak discharge from NS in constant precipitation amount condition (415.3 and 393.8 mm, respectively) of snow fall period in the two successive hydrologic years points to the effects of another variable. Melting process is among the effective variables on springs discharge (Malík and Vojtková 2012; Lo Russo et al, 2015) that changes in time and intensity. Snowmelt starts with 20-day delay in 2016; however, it melts more intensely in comparison to 2015 probably due to higher air

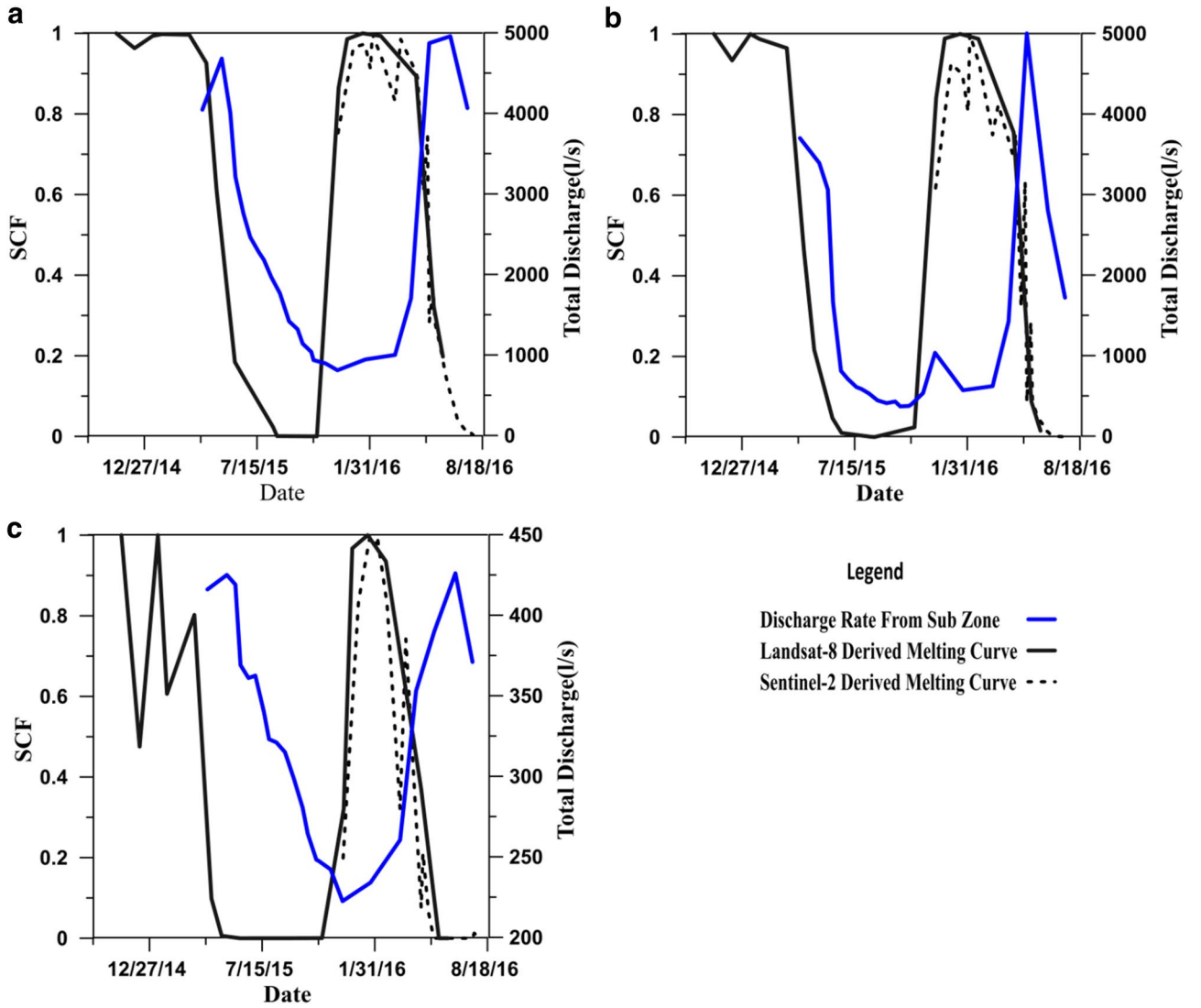

Fig. 7 Snowmelt curves for the sub-zones of the Lasem basin (**a**) HNFS, (**b**) LNSF, and (**c**) SFS

temperature. The more intense snowmelt in 2015–2016 in comparison to 2014–2015 results in nearly 15% raise of peak discharge of spring's water feeding by the NFS. Conversely, there is no such noticeable changes in peak discharge on karst springs fed by the dominance of SFS. This may be explained by the dominance of diffuse flow regime in this group of springs.

Considering time lag for transferring the peak melt to the karst springs shows nearly the same duration (20–35 days) for springs predominantly fed by NFS which is lower than feeding springs by the SFS (70–80 days). The quite same transient time for the peak melt in both lower and higher elevated NFS probably results from the same degree of karstification in these subdomains while longer transient time (70–80 days) in SFS points to the lower karstification. Recession curve analysis of the karst springs in the area showed that the springs fed by SFS have lower karstification degree and dominant form of the flow is diffused, while those fed by NFS are highly karstified and dominated by conduit flow regime (Shamsi et al. 2019). The lower time lag of springs fed by NFS proves the higher karstification degree in comparison to those fed by SFS subdomain. This highlights the important role of snow preservation on the carbonate landscape as observed in this area in the same formation that leads to the higher karstification degree in NFS (Shamsi et al. 2019).

Conclusions

Remote sensing is a beneficial tool for monitoring SCA and variations of snowmelt process especially for remote and high-elevated mountains where suffer from the lack of

data monitoring instruments. Since the spatial and temporal resolutions are important for small-scale SCA monitoring, using different datasets makes it possible to cover the gaps by other dataset. Investigation of snowmelt and its effects on groundwater is crucial for water resources management and forecasting the spring snowmelt flooding. This research investigated the SCA and snowmelt process at the Lasem area using Landsat-8 and Sentinel-2 satellites datasets. General consistency between the total snow cover from Landsat-8 and Sentinel-2 images highlights the robustness of the method. However, some differences were observed due to the different spatial resolutions. The higher temporal and spatial resolution of Sentinel-2 made it possible to monitor the melting processes with more details than Landsat-8, specifically for early melt in SFS.

Generally, spatial distribution of the SCA during the cold season remains near the maximum at higher elevated parts and NFS, while it somehow fluctuates in SFS and lower elevated parts. However, some changes are possible due to early melt resulting from short-term meteorological conditions and slope direction effect.

Subdomain-based snow cover depletion curve showed that melting process timing and intensity varied from year to year; these variations have a direct proportional controlling role on springs discharge in karst landscapes.

In the study area, the majority of snowpack melts in May; however, in higher elevated NFS, it continued till June. Comparison of the snowmelt process results in two successive water years (2014–2015 and 2015–2016) indicates there is a distinct change in timing and slope of the melting curve in a NFS. The higher slope of the melting curve during 2015–2016 indicates the higher intensity of melting processes in spring 2016, which leads to the increasing peak discharge in 2016 in comparison to 2015 by 15%. Noticeable raise in peak flow discharge of NFS karst springs (15%) in 2016 while the equivalent water of accumulated snow for two succeeding years are nearly the same (415.3 and 393.8 mm, respectively) with having different melting intensity shows the effects of melting process on karst springs discharge. The springs recharged by dominant SFS show no distinct change in time and intensity of the melting curves in two successive years. Although the melting starts earlier in springs with dominant SFS, their discharges show no noticeable reaction to the snowmelt process in comparison to the springs with dominant NFS. Faster transmitting time (20–35 days) of the peak snowmelt to the springs in NFS with more sensitivity of their discharges in comparison to discharging karst springs from SFS with longer transmitting time of peak snowmelt (70–80 days) and negligible change in springs discharge, indicating a higher degree of karstification in NFS.

Using two different datasets will be beneficial to fill the gaps resulting from unsuitable images of one satellite with the results from the other satellite. Increasing availability of remote sensing data with appropriate spatial and temporal resolution (e.g., Sentinel-2A) allows obtaining more reliable data about SCA and snow melting processes.

Acknowledgements The authors would like to thank the anonymous reviewers for the constructive, insightful comments and suggestions.

References

Bakalowicz M (2005) Karst groundwater: a challenge for new resources. Hydrogeol J 13(1):148–160. https://doi.org/10.1007/s10040-004-0402-9

Barnett TP, Adam JC, Lettenmaier DP (2005) Potential impacts of a warming climate on water availability in snow-dominated regions. Nature 438(7066):303–309. https://doi.org/10.1038/nature04141

Berberian M, Yeats RS (1999) Patterns of historical earthquake rupture in the Iranian Plateau. Bull Seismol Soc Am 89(1):120–139

Bonacci O (1993) Karst springs hydrographs as indicators of karst aquifers. Hydrol Sci J 38(1–2):51–62

Bonacci O, Andrić I (2015) Karst spring catchment: an example from Dinaric karst. Environ Earth Sci 74(7):6211–6223. https://doi.org/10.1007/s12665-015-4644-8

Bormann KJ, McCabe MH, Evans JP (2012) Satellite based observations for seasonal snow cover detection and characterization in Australia. Remote Sens Environ 123:57–71. https://doi.org/10.1016/j.rse.2012.03.003

Brown ME, Racoviteanu AE, Tarboton DG, Gupta AS, Nigro J, Policelli F, Tokar S (2014) An integrated modeling system for estimating glacier and snow melt driven stream flow from remote sensing and earth system data products in the Himalayas. J Hydrol 519:1859–1869. https://doi.org/10.1016/j.jhydrol.2014.09.050

Crawford CJ, Manson SM, Bauer ME, Hall DK (2013) Multi-temporal snow cover mapping in mountainous terrain for Landsat climate data record development. Remote Sens Environ 135:224–233. https://doi.org/10.1016/j.rse.2013.04.004

Deng Y, Flerchinger GN, Cooley KR (1994) Impacts of spatially and temporally varying snowmelt on subsurface flow in a mountainous watershed: 2. Subsurf Process Hydrol Sci J 39(5):521–533. https://doi.org/10.1080/02626669409492772

Dietz AJ, KuenzerC GessnerU, Dech S (2012) Remote sensing of snow—a review of available methods. Int J Remote Sens 33(13):4094–4134. https://doi.org/10.1080/01431161.2011.640964

Dietz A, Conrad C, Kuenzer C, Gesell G, Dech S (2014) Identifying changing snow cover characteristics in Central Asia between 1986 and 2014 from remote sensing data. Remote Sens 6(12):12752–12775. https://doi.org/10.3390/rs61212752

Dozier J (1989) Spectral signature of alpine snow cover from the landsat thematic mapper. Remote Sens Environ 28:9–22. https://doi.org/10.1016/0034-4257(89)90101-6

Egbers R (2016) Sentinel-2 data processing and identifying glacial features in Sentinel-2 imagery. BSc Thesis, TU Delft, University of Technology, Netherlands

Emami MH, Babakhani A (1997) Geological map of Damavand. Geological Survey of Iran, scale 1:100,000

European Space Agency (ESA) (2016) https://sentinel.esa.int/web/sentinel/sentinel-dataaccess. Accessed Sept 2016

Earth Explorer (2016) https://earthexplorer.usgs.gov. Accessed Sept 2016

Fassnacht SR, Sexstone GA, Kashipazha AH, López-Moreno JI, Jasinski MF, Kampf SK, Von Thaden BC (2016) Deriving snow-cover depletion curves for different spatial scales from remote sensing

and snow telemetry data. Hydrol Process 30(11):1708–1717. https://doi.org/10.1002/hyp.10730
Fassnacht SR, López-Moreno JI, Ma C, Weber AN, Pfohl AKD, Kampf SK, Kappas M (2017) Spatio-temporal snowmelt variability across the headwaters of the Southern Rocky Mountains. Front Earth Sci 11(3):505–514. https://doi.org/10.1007/s11707-017-0641-4
Fiorillo F, Guadagno FM (2012) Long karst spring discharge time series and droughts occurrence in southern Italy. Environ Earth Sci 65:2273–2283. https://doi.org/10.1007/s12665-011-1495-9
Flerchinger GN, Cooley KR, Ralston DR (1992) Groundwater response to snowmelt in a mountainous watershed. J Hydrol 133:293–311. https://doi.org/10.1016/0022-1694(92)90260-3
Gusev YM, Nasonova ON (2014) Application of a technique for scenario prediction of climate change impact on the water balance components of northern river basins. J Hydrol Hydromech 62:1–12. https://doi.org/10.2478/johh-2014-0025
Hall DK, Riggs GA, Salomonson VV (1995) Development of methods for mapping global snow cover using moderate resolution imaging spectroradiometer data. Remote Sens Environ 54:127–140. https://doi.org/10.1016/0034-4257(95)00137-P
Hall DK, Riggs GA, Salomonson VV, DiGirolamo NE, Bayr KJ (2002) MODIS snowcover products. Remote Sens Environ 83(1–2):181–194. https://doi.org/10.1016/S00344257(02)00095-0
Hall DK, Foster JL, DiGirolamo NE, Riggs GA (2012) Snow cover, snowmelt timing and stream power in the Wind River Range. Wyo Geomorphol 137(1):87–93. https://doi.org/10.1016/j.geomorph.2010.11.011
Hall DK, Crawford CJ, DiGirolamo NE, Riggs GA, Foster JL (2015) Detection of earlier snowmelt in the Wind River Range, Wyoming, using Landsat imagery, 1972–2013. Remote Sens Environ 162:45–54. https://doi.org/10.1016/j.rse.2015.01.032
Hartmann A, Gleeson T, Wada Y, Wagener T (2017) Enhanced groundwater recharge rates and altered recharge sensitivity to climate variability through subsurface heterogeneity. Proc Natl Acad Sci USA 114(11):2842–2847. https://doi.org/10.1073/pnas.1614941114
Kääb A, Winsvold S, Altena B, Nuth C, Nagler T, Wuite J (2016) Glacier remote sensing using Sentinel-2. Part I: radiometric and geometric performance, and application to ice velocity. Remote Sens 8(7):598. https://doi.org/10.3390/rs8070598
Kavousi A, Raeisi E (2015) Estimation of groundwater mean residence time in unconfined karst aquifers using recession curves. J Cave Karst Stud 77(2):108–119. https://doi.org/10.4311/2014ES0106
Khalili A (1973) Precipitation patterns of central Elburz. Archiv für Meteorologie, Geophysik und Bioklimatologie, Serie B 21(2–3):215–232
Lo Russo S, Amanzio G, Ghione R, De Maio M (2015) Recession hydrographs and time series analysis of springs monitoring data: application on porous and shallow aquifers in mountain areas (Aosta Valley). Environ Earth Sci 73(11):7415–7434. https://doi.org/10.1007/s12665-014-3916-z
Macander MJ, Swingley CS, Joly K, Raynolds MK (2015) Landsat-based snow persistence map for northwest Alaska. Remote Sens Environ 163:23–31. https://doi.org/10.1016/j.rse.2015.02.028
MacDonald LH (1987) Forest harvest, snowmelt and stream flow in the central Sierra Nevada. Forest hydrology and watershed management. Vancouver Symp., 9–22 August 1987, Vancouver, B.C. IAHS-AISH, Wallingford, Publ 167:273–283
Malík P, Vojtková S (2012) Use of recession-curve analysis for estimation of karstification degree and its application in assessing overflow/underflow conditions in closely spaced karstic springs. Environ Earth Sci 65(8):2245–2257. https://doi.org/10.1007/s12665-012-1596-0
Miao J, Liu G, Cao B, Hao Y, Chen J, Yeh TCJ (2014) Identification of strong karst groundwater runoff belt by cross wavelet transform. Water Resour Manag 28:2903–2916. https://doi.org/10.1007/s11269-014-0645-8
Padilla A, Pulido-Bosch A, Mangin A (1994) Relative importance of baseflow and quick flow from hydrographs of karst spring. Groundwater 32(2):267–277. https://doi.org/10.1111/j.17456584.1994.tb00641.x
Poulain A, Rochez G, Bonniver I, Hallet V (2015) Stalactite drip-water monitoring and tracer tests approach to assess hydrogeologic behavior of karst vadose zone: case study of Han-sur-Lesse (Belgium). Environ Earth Sci Environ Earth Sci 74(12):7685–7697. https://doi.org/10.1007/s12665-015-4696-9
Radulovic M, Stevanovic Z, Radulovic M (2012) A new approach in assessing recharge of highly karstified terrains-Montenegro case studies. Environ Earth Sci 65(8):2221–2230. https://doi.org/10.1007/s12665-011-1378-0
Rango A, Wergin WP, Erbe EF (1996) Snow crystal imaging using scanning electron microscopy: part II—metamorphosed snow. Hydrol Sci J 41(2):235–250. https://doi.org/10.1080/02626669609491495
Rittger K, Painter TH, Dozier J (2012) Assessment of methods for mapping snow cover from MODIS. Adv Water Resour 51:367–380. https://doi.org/10.1016/j.advwatres.2012.03.002
Schmieder J, Hanzer F, Marke T, Garvelmann J, Warscher M, Kunstmann H, Strasser U (2016) The importance of snowmelt spatiotemporal variability for isotope-based hydrograph separation in a high-elevation catchment. Hydrol Earth Syst Sci 20(12):5015–5033. https://doi.org/10.5194/hess-20-5015-2016
Shamsi A, Karami GH, Taheri A (2019) Recession curve analysis of major karstic springs at the Lasem area (north of Iran). Carbonates Evaporites 2019:1–12. https://doi.org/10.1007/s13146-019-00501-7
Smith T, Bookhagen B, Rheinwalt A (2017) Spatiotemporal patterns of High Mountain Asia's snowmelt season identified with an automated snowmelt detection algorithm, 1987–2016. Cryosphere 11(5):2329–2343. https://doi.org/10.5194/tc-11-2329-2017
Tedesco M, Parrinello T, Webb C, Markus T (2014) Remote sensing missions and the cryosphere. In: Tedesco M (ed) Remote sensing of the cryosphere. Wiley, Chichester, pp 382–392
White WB (2007) A brief history of karst hydrogeology: contributions of the NSS. J Cave Karst Stud 69(1):13–26